# Proton NMR Assignments and Magnetic Axes Orientations for Wild-Type Yeast Iso-1-ferricytochrome *c* Free in Solution and Bound to Cytochrome *c* Peroxidase†

Steven F. Sukits,‡ James E. Erman,§ and James D. Satterlee*,‡

*Department of Chemistry, Washington State University, Pullman, Washington 99164-4630, and Department of Chemistry, Northern Illinois University, DeKalb, Illinois 60115*

*Received January 13, 1997; Revised Manuscript Received March 6, 1997*⊗

ABSTRACT: Extensive proton hyperfine-shifted resonance assignments have been made for wild-type yeast iso-1-ferricytochrome *c* when it is free in solution and when it is noncovalently complexed to resting state cytochrome *c* peroxidase. Complete heme proton resonance assignments were made for free iso-1-ferricytochrome *c*, while for CcP-complexed iso-1-ferricytochrome *c*, 70% of heme proton assignments were made. Additional proton resonance assignments were made for hyperfine-shifted protons of amino acids near the heme. These assignments allowed identification of the most extensive set of complex-induced proton shifts yet reported for CcP/cytochrome *c* complexes. Several purely dipolar-shifted resonances from heme vicinity amino acid protons were also assigned in both free and complexed iso-1-ferricyt *c*. Both sets of resonance assignments allowed assessment of the origin of proton complex-induced shifts. Using the assigned dipolar-shifted proton resonances as a basis, the orientations of the principal axis systems of the paramagnetic susceptibility tensors for free and cytochrome *c* peroxidase-bound iso-1-ferricytochrome *c* were elucidated. The results indicated that the iso-1-ferricytochrome *c* magnetic axis system orientation shifts significantly upon complex formation. The direction of the complex-induced shifts for heme proton resonances is largely accounted for by the magnetic anisotropy changes. However, analysis of heme complex-induced shifts also reveals local changes in magnetic environment for two heme substituents, presumably through a specific structure change.

Cytochrome *c* (cyt *c*; 12.5 kDa) and cytochrome *c* peroxidase (CcP; 34.2 kDa) are water soluble redox proteins found in yeast mitochondria. CcP catalyzes the oxidation of ferrocyt *c* in a reaction that is believed to involve intramolecular electron transfer within a complex of the two proteins. Recently, there has been disagreement as to whether the active electron transfer complex has a stoichiometry of 1:2 (CcP/cyt *c*) (Stemp & Hoffman, 1993; Zhou & Hoffman, 1994; Mauk et al., 1994) or 1:1 (Pelletier & Kraut, 1992; Pappa & Poulos, 1995; Miller et al., 1996). However, all studies so far published reveal that at an ionic strength corresponding to that of the mitochondrial intermembrane space only a 1:1 complex is detectable (Stemp & Hoffman, 1993; Zhou & Hoffman, 1994; Mauk et al., 1994). Those data, combined with kinetic characterization of a 1:1 complex showing it to be kinetically competent (Miller et al., 1996), imply that a 1:1 complex is functional, thereby justifying further characterization.

A noncovalent 1:1 cyt *c*/CcP complex forms spontaneously at low ionic strengths. In addition to its specific relevance to CcP function and mitochondrial redox chemistry, this complex provides a good system in which to test methods for studying metalloenzyme protein/protein complexes by NMR because its overall size (46.7 kDa) is a substantial challenge to current NMR capabilities. The complex and both proteins are water soluble, making them amenable to the same types of solution state studies, which can then be compared.

In this paper, we report detailed proton hyperfine resonance assignments for wild-type yeast iso-1-ferricyt *c* in the free state (in solution) and complexed to resting state CcP. We have used both proteins in their paramagnetic ferric states ($Fe^{3+}$). In both free and complexed environments, wild-type iso-1-ferricyt *c* is low-spin and has a total of one unpaired electron spin ($S = {}^1/_2$), while CcP is in the high-spin $S = {}^5/_2$ state. With respect to the proposed catalytic cycle (Poulos & Finzel, 1984; Neuvo et al., 1993; Hahm et al., 1994; Liu et al., 1995; Matthis et al., 1995a,b), this complex mimics the one that results after the final electron transfer from ferrocytochrome *c* to CcP, prior to complex dissociation (the so-called "product complex"). Resting state CcP was chosen over low-spin CcPCN in this study not only for biological accuracy but also because of its magnetically isotropic orbital ground state, which produces broad and highly shifted proton hyperfine resonances that do not interfere with detection of the narrower, less highly shifted ferricyt *c* resonances.

Previously, we have shown that it is possible to completely assign the heme protons and other significantly hyperfine-shifted protons in a homogeneous solution of free tuna ferricyt *c* using appropriate two-dimensional NMR methods (Sukits & Satterlee, 1996). The results presented here extend

†This work was supported by the National Institutes of Health (GM 47645 and GM 45986; J.D.S.) and the National Science Foundation (MCB 9513047; J.E.E.). This study also made use of the National Magnetic Resonance Facility at Madison, which is supported by NIH Grant RR02301 from the Biomedical Research Technology Program, National Center for Research Resources. Equipment in the facility was purchased with funds from the University of Wisconsin, the NSF Biological Instrumentation Program (DMB-8415048), the NSF Academic Research Instrumentation Program (BIR-9214394), the NIH Biomedical Research Technology Program (RR02301), and the NIH Shared Instrumentation Program.

* Address correspondence to Professor Satterlee. E-mail: hemeteam@cosy.chem.wsu.edu. Phone: 509-335-8620. Fax: 509-335-8867.

‡ Washington State University.

§ Northern Illinois University.

⊗ Abstract published in *Advance ACS Abstracts,* April 15, 1997.

S0006-2960(97)00072-X CCC: $14.00 

that work and demonstrate the benefit of using such an approach to study larger paramagnetic complexes. We have achieved complete heme proton resonance assignments and substantial assignments of hyperfine-shifted protons of heme site amino acids for the free form of wild-type iso-1-ferricyt *c* (12.5 kDa). We have also assigned over 70% of the iso-1-ferricyt *c* heme protons and many hyperfine-shifted proton resonances of iso-1 heme site amino acids in the 46.7 kDa 1:1 noncovalent complex. Many of these newly identified hyperfine-shifted proton resonances exhibit complex-induced shifts greater than 200 Hz, providing a more comprehensive mapping of the effect of complex formation upon the iso-1 heme pocket. As a means of analyzing the origin of these complex-induced proton resonance shifts, the orientations of the paramagnetic susceptibility tensor axis systems were determined for wild-type yeast iso-1-ferricyt *c* both free (in solution) and in the 1:1 noncovalent complex with CcP.

## MATERIALS AND METHODS

*Sample Preparation.* Wild-type yeast *(Saccharomyces cerevisiae*) iso-1-cytochrome *c* was separated from commercial (Sigma) preparations as reported by Moench and Satterlee (1989). The purified fraction was washed in an Amicon ultrafiltration device with deionized water and lyophilized. Yeast cytochrome *c* peroxidase was isolated and purified as previously described (Vitello et al., 1990).

*Proton Resonance Assignments for Yeast Iso-1-ferricyt c.* Wild-type yeast iso-1-ferricyt *c* NMR samples for proton assignments were prepared as previously described (Sukits & Satterlee, 1996). NMR data were collected at Washington State University on a VXR500S spectrometer operating at a nominal proton frequency of 500 MHz and at NMR Facility at Madison (University of Wisconsin) on a DMX750 spectrometer operating at a nominal proton frequency of 750.13 MHz. DEFT−NOESY (Kao & Hruby, 1986) experiments were performed at 25 °C with a relaxation delay ($\tau$) of 150 ms and mixing times of 5, 7, 10, 15, 25, 35, 45, and 60 ms. CLEAN−TOCSY (Griesinger et al., 1988) experiments were performed at 25 °C with a repetition rate of 2 $s^{-1}$ and mixing times of 10, 15, 30, and 50 ms utilizing an MLEV-17 mixing scheme. A 56.7 $\mu$s delay was used to suppress relaxation-allowed coherence transfer (RACT) (Bertini et al., 1993; Qin et al., 1993), and a 2 ms trim pulse was applied prior to the spin lock. The residual $^1H_2O$ peak was suppressed for 250 ms during the relaxation delay time ($d_1$) .

Phase sensitive spectra were collected with a spectral width of 40 000 Hz for the DEFT−NOESY experiments and 13 227.5 Hz for the CLEAN−TOCSY experiments, 2048 hypercomplex data points in the $F_2$ dimension, 512 $t_1$ increments, and 128 scans per block. All phase sensitive spectra were acquired using the hypercomplex method of States (1992). All two-dimensional data were processed on a Silicon Graphics Indigo 2 workstation using the Felix 95.0 program

*Proton Resonance Assignments for the Cyt c/CcP Complex.* CcP was solubilized in a 100 mM potassium phosphate/100 mM potassium chloride/99.9% $D_2O$ buffer at pH 6.9 (uncorrected). CcP and wild-type yeast iso-1-ferricyt *c* were mixed at a 1:1 mole ratio in a 10 mM potassium phosphate solution (pH 6.9) in order to form the noncovalent complex. NMR data were collected in a fashion similar to that employed for ferricyt *c* with the following exceptions. The relaxation delay ($\tau$) in the DEFT−NOESY experiment was reduced to 120 ms, and 224 scans per block were collected instead of 128.

*Magnetic Axes Determination.* The magnetic axes were determined as described in detail previously (Emerson & La Mar, 1990; Rajarathnam et al., 1992; La Mar et al., 1995) using programs kindly provided by G. N. La Mar. Experimental dipolar shifts of amino acids dispersed around the heme were used as input to search for the Euler rotation angles, $R(\alpha,\beta,\gamma)$, that transform the molecular pseudosymmetry coordinates, $x',y',z'$ or $r,\theta',\phi'$ (readily obtained from crystal coordinates), into magnetic axes, $x,y,z$ (Figure 1A), by minimizing the following error function:

$$F/n = \sum^{n} |\delta_{dip}(\text{obs}) - \delta_{dip}(\text{calc})F(\alpha,\beta,\gamma)|^2 \qquad (1)$$

where

$$\delta_{dip}(\text{calc}) = -\frac{1}{3N}[\Delta\chi_{ax}(3\cos^2\theta' - 1)r^{-3} + {}^3/_2\Delta\chi_{rh}\sin\theta'\cos 2\phi' r^{-3}] \qquad (2)$$

and

$$\delta_{dip}(\text{obs}) = \delta_{DSS} - \delta_{dia} \qquad (3)$$

$\Delta\chi_{ax}$ and $\Delta\chi_{rh}$ are axial and rhombic susceptibility anisotropies, respectively. We note that protons of amino acids not directly bonded to the heme iron ion can only experience a dipolar paramagnetic contribution to their observed shifts (Satterlee, 1986). $\delta_{dia}$ is the experimentally determined proton shift in the ferrous form of wild-type yeast iso-1-cyt *c* (S. F. Sukits and J. D. Satterlee, unpublished) or, for protons whose $\delta_{dia}$ values were not experimentally available, calculated by the equation

$$\delta_{dia} = \delta_{sec} - \delta_{rc} \qquad (4)$$

where $\delta_{sec}$ is the shift of an amino acid proton typical for α-helices (Wishart et al., 1991) and $\delta_{rc}$ is the heme-induced ring current shift of the proton based on the crystal structure coordinates calculated using the eight-loop model (Cross & Wright, 1985). Minimizing the error function *F/n* in eq 1 was performed over three parameters, α, $\beta$, and $\gamma$, using available $\Delta\chi_{ax}$ and $\Delta\chi_{rh}$ or extended to all five parameters to yield both the Euler angles and anisotropies (Rajarathnam et al., 1992).

*Structure Coordinates.* Two crystal structures of wild-type yeast iso-1-cytochrome *c* have been published: the ferrous form (Louie & Brayer, 1990) and the ferric form as part of the CcP/ferricyt *c* complex (Pelletier & Kraut, 1992). The coordinates for these two structures were retrieved from the Protein Data Bank (Bernstein et al., 1977) and processed on a Silicon Graphics Indigo 2 workstation using InsightII (Biosym/MSI).

## RESULTS

*Proton Resonance Assignments for Heme and Active Site Amino Acids.* In this work, we have employed wild-type yeast iso-1-cyt *c* because it is the naturally occurring protein in yeast mitochondria. Similar proton resonance assignments (albeit, using different methods) have been published for the

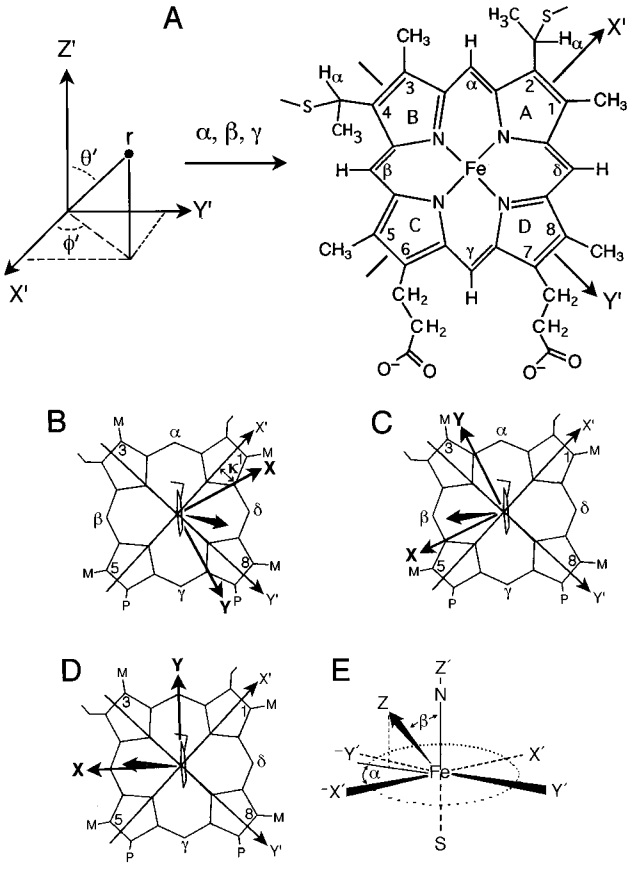


FIGURE 1: (A) Generalized search strategy for a magnetic axis system orientation, definition of molecule-based initial axis system, and detailed Fischer labeling for heme *c* used in this work. Panel B represents the result of the Euler angle five-parameter search using dipolar-shifted protons for iso-1-ferricyt *c* free in solution. Panel C represents the result of the Euler angle three-parameter search using dipolar-shifted protons for iso-1-ferricyt *c* complexed to CcP. Panel D represents the "optimal" magnetic axis system orientation that accounts for the pattern of heme dipolar complex-induced shifts. The molecular structure frameworks shown in panels A−D were derived from edited crystal structures showing heme *c* viewed from the His18 side, approximately perpendicular to the heme, along the Fe−N(His18) bond. The His18 side chain imidazole ring is in the foreground. Shown in panels B−D are the heme peripheral substituents (M = methyl; P = propionic acid), as well as the molecular symmetry axes $X'$ and $Y'$ which were used at the start of the magnetic axis search, and the final magnetic axis orientations $X$ ($\chi_{xx}$) and $Y$ ($\chi_{yy}$). The $Z$ ($\chi_{zz}$) axis is not labeled but is depicted by a heavy arrow drawn in perspective emanating from the heme center, directed toward the viewer. The Euler angle $\kappa$ is defined in panel B. Panel E is a tilted, edgewise view of the heme plane defined by $X'$ and $Y'$ showing ligation of the heme Fe ion to the N(His18) and S(Met80) and defining the remaining two Euler angles. The $\beta$ angle measures the deviation of $Z$ ($\chi_{zz}$) from the heme normal defined by the Fe−N(His18) bond ($Z'$). The angle between the projection of $Z$ onto the $X'/Y'$ plane and the $-X'$ axis defines $\alpha$.

C102T and C102S variants of iso-1 (Gao et al., 1991, 1992; Baistrocchi et al., 1996). On the basis of structure and spectroscopy comparisons with wild-type iso-1-cyt *c*, the position-102 variants of iso-1 have come to be regarded in some circles as the *de facto* "native" protein (Pielak et al., 1988; Berghuis & Brayer, 1992; Baistrocchi et al., 1996), but those variants are not the naturally occurring redox partners of CcP, which is why we have chosen to study wild-type iso-1, despite its more complicated solution chemistry (Satterlee et al., 1988; Moench & Satterlee, 1989; Moench et al., 1992).

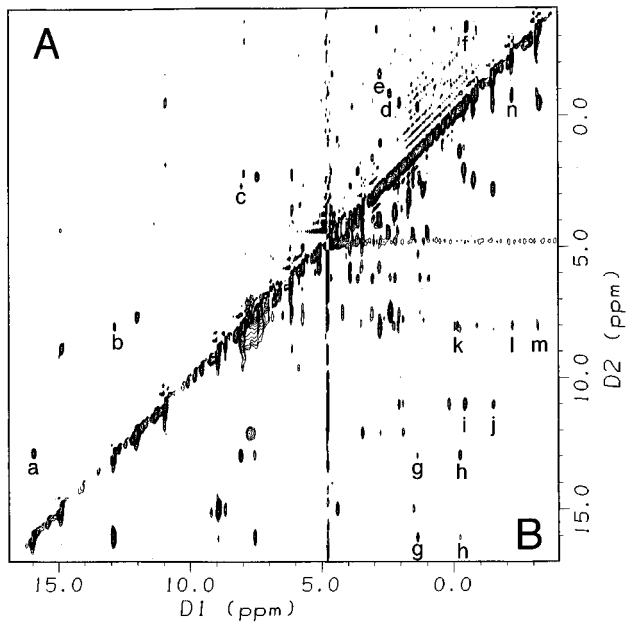


FIGURE 2: Split diagonal 500 MHz contour plot of a $^1$H DEFT−NOESY spectrum of yeast iso-1-ferricytochrome *c* in 99.9% $D_2O$ and 10 mM potassium phosphate buffer at pH 6.9 collected at 25 °C. (A) a 5 ms mixing time experiment showing short range NOEs and (B) a 25 ms mixing time experiment. Cross-peak assignments are described in the text.

The heme *c* structure and modified Fischer (IUPAC, 1988) labeling scheme employed in this work are shown in Figure 1A. Panels B−D of Figure 1 define the Euler angles that result from our magnetic axis determinations and indicate the structural elements used in these experiments (*vide infra*).

Figure 2 is a split-diagonal contour plot of homonuclear proton DEFT−NOESY experiments. Figure 2A shows an experiment conducted with a 5 ms mixing time, and Figure 2B is an experiment that employed a 25 ms mixing time. Both parts of this figure show labeled cross-peaks indicating some of our heme and amino acid proton hyperfine resonance assignments. The short mixing time DEFT−NOESY in Figure 2A was used to establish primary NOEs and identify connectivities between protons that are very close in space such as the heme propionate geminal proton pair, 7α−7α (cross-peak a), and the heme propionate geminal proton pair, 6α−6α (cross-peak e), and also between protons of neighboring substituents on the heme, such as 7α−$\gamma_{meso}$ protons (cross-peak b), 6α−$\gamma_{meso}$ protons (cross-peak c), and 2CH−$\alpha_{meso}$ protons (cross-peak d). It also shows intraresidue proton connectivities among amino acid resonances, such as Leu68δ-Leu68δ (cross-peak f). In Figure 2B, longer range NOEs are observed. The results stereochemically define several protons, such as the heme propionate 7α closest to the 8-$CH_3$ in the crystal structure (Louie & Brayer, 1990), which is identified by NOEs to the 8-$CH_3$ resonance as well as to resonances of its geminal partner, 7α, and to both 7βs (cross-peaks g and h). The heme propionate 7α proton closest to the $\gamma_{meso}$ in the crystal structure shows NOEs to the $\gamma_{meso}$ and both 7βs. On the basis of NOE intensity, the heme propionate 7βs are stereospecifically assigned. The previously assigned heme 5-$CH_3$ proton shows NOEs to both the heme $\beta_{meso}$ proton (cross-peak i) and the heme propionate 6α proton (cross-peak j). The heme 1-$CH_3$ proton was identified on the basis of NOEs from the heme 2-$CH_3$ (cross-peak l), $\delta_{meso}$ (cross-peak k), and Leu68δ (cross-peak m)

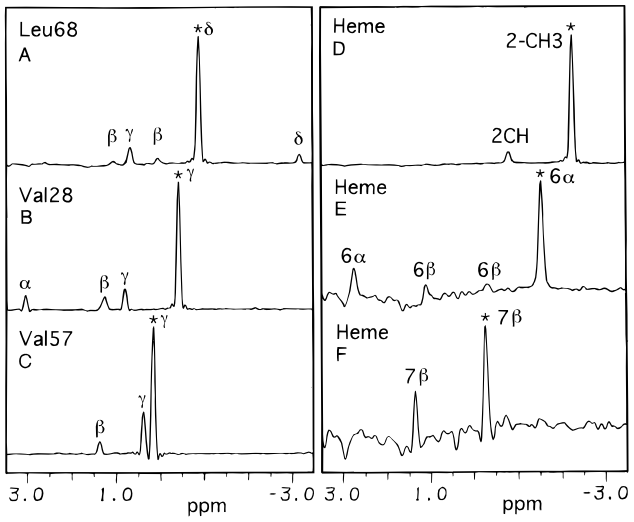


FIGURE 3: $F_2$ slices of the 500 MHz $^1$H NMR CLEAN−TOCSY spectrum of yeast iso-1-ferricytochrome *c* in 99.9% $D_2O$ and 10 mM potassium phosphate buffer at pH 6.9 collected at 25 °C. Individual boxes show different spin systems, as labeled on the figure. All of the spectra were collected with an isotropic mixing time of 50 ms except for the heme 6-propionate spin system (E) which was acquired with a 15 ms mixing time. The asterisk (*) on each of the one-dimensional slices indicates the diagonal peak.

protons. In addition, the connectivity between the heme 2-$CH_3$ and the heme 2-CH (cross-peak n) protons can be found in Figure 2B.

Resonance assignments from DEFT−NOESY experiments were confirmed using the CLEAN−TOCSY scalar coupling experiment. Figure 3 shows examples of one-dimensional slices of some of this data. Figure 3A shows the Leu68 spin system. This 50 ms mixing time CLEAN−TOCSY reveals the correlations of the Leu68 $\delta$-$CH_3$ to the $\delta'$-$CH_3$, $\gamma$-H, and both $\beta$-Hs. Parts B and C of Figure 3 show scalar correlations for two of the Val spin systems. For example, the correlation of the Val28 $\gamma$-H to the rest of the spin system ($\gamma$-, $\beta$-, and α-Hs) is shown in Figure 3B. Figure 3 also shows scalar correlation for some of the heme substituents: (3D) 2-$CH_3$−2-CH, (3E) 6α−6α and 6α−6$\beta$, and (3F) 7$\beta$−7$\beta$ protons. The asterisk (*) in each panel denotes the diagonal cross-peak, and all spectra were acquired with an isotropic mixing time of 50 ms except for Figure 3E, which was acquired with an isotropic mixing time of 15 ms. Complete heme proton assignments (Table 1) and several hyperfine-shifted amino acid proton assignments (Table 2) were made by this strategy which has been previously detailed for tuna ferricyt *c* (Sukits & Satterlee, 1996).

*Active Site Amino Acids and Heme Resonance Assignments of Yeast Iso-1-ferricyt c Complexed to CcP.* Proton resonance assignments for over 70% of the heme protons and for nine dipolar-shifted amino acid protons have been made. The substantially increased resonance density in the "diamagnetic" (−1 to 11 ppm) region for this 46.7 kDa complex (∼4000 protons) compared to that for the 12.5 kDa ferricyt *c* (∼1000 protons) is a complicating factor in the assignment strategy. However, assignments were achieved by taking advantage of the more rapid nuclear relaxation rates of highly hyperfine-shifted resonances in DEFT−NOESY experiments.

Some feeling for how intense the diamagnetic envelope of resonance density can become is given by Figure 4, a split-diagonal presentation of contour plots. Figure 4A is the spectrum obtained with a 7 ms mixing time showing

Table 1: Proton Resonance Assignments of Iso-1-ferricytochrome *c* Free and Bound to CcP, and Their Difference, Which Is the Complex-Induced Shift

| resonance | free (ppm) | bound (ppm) | difference (Hz)[a] |
|---|---|---|---|
| 1-$CH_3$ | 8.01 | 8.47 | 230 |
| 3-$CH_3$ | 31.33 | 33.36 | 1015 |
| 5-$CH_3$ | 11.02 | 10.57 | −225 |
| 8-$CH_3$ | 34.81 | 35.13 | 160 |
| α-meso | 2.41 | 2.91 | 250 |
| $\beta$-meso | −0.44 | −0.57 | −80 |
| $\gamma$-meso | 8.07 | | |
| $\delta$-meso | 2.25 | 2.10 | −75 |
| 2-CH | −0.74 | −0.58 | 80 |
| 2-$CH_3$ | −2.24 | −2.16 | 40 |
| 4-CH | 2.07 | | |
| 4-$CH_3$ | 2.86 | 3.30 | 220 |
| 6α | −1.51 | −1.95 | −220 |
| 6α | 2.80 | | |
| 6$\beta$ | 1.12 | | |
| 6$\beta$ | −0.51 | −0.21 | 150 |
| 7α | 16.08 | 15.53 | −275 |
| 7α | 12.91 | 13.52 | 305 |
| 7$\beta$ | 1.36 | | |
| 7$\beta$ | −0.25 | | |
| Pro30$\delta$ | −5.56 | −5.09 | 235 |
| Pro30$\delta$ | −1.43 | −1.39 | 20 |
| Gly29α | −3.23 | −3.33 | −50 |
| Gly29α | −0.51 | −0.39 | 60 |
| Leu68$\delta$ | −3.11 | −3.53 | −210 |
| Leu68$\delta$ | −0.88 | −0.97 | −45 |
| Phe82$\delta$ | 6.15 | 6.46 | 155 |
| Ile35$\gamma$ | 0.96 | 1.01 | 25 |
| Trp59$\zeta$ | 7.54 | 7.59 | 25 |

[a] At 500 MHz.

Table 2: Assignments for Hyperfine-Shifted Amino Acid Protons for Iso-1-ferricytochrome *c* Free in Solution

| resonance | free (ppm) | resonance | free (ppm) |
|---|---|---|---|
| Leu15α | 6.12 | Ile35$\gamma$ | 0.96 |
| Leu15$\beta$ | 2.53 | Tyr46$\epsilon$ | 5.70 |
| Leu15$\beta$ | 2.18 | Val57α | 4.13 |
| Leu15$\gamma$ | 2.39 | Val57$\beta$ | 1.37 |
| Thr19α | 6.35 | Val57$\gamma$ | 0.39 |
| Thr19$\beta$ | 5.46 | Val57$\gamma$ | 0.15 |
| Val28α | 3.05 | Leu68$\delta$ | −3.11 |
| Val28$\beta$ | 1.26 | Leu68$\delta$ | −0.88 |
| Val28$\gamma$ | 0.81 | Leu68$\gamma$ | 0.70 |
| Val28$\gamma$ | −0.43 | Leu68$\beta$ | 0.06 |
| Gly29α | −3.28 | Leu68α | 2.90 |
| Gly29α | −0.46 | Thr78α | 5.24 |
| Pro30$\delta$ | −5.56 | Thr78$\beta$ | 5.83 |
| Pro30$\delta$ | −1.43 | Thr78$\gamma$ | 3.42 |
| Pro30$\gamma$ | −0.43 | Ala81α | 5.19 |
| Pro30$\gamma$ | −0.79 | Ala81$\beta$ | 1.32 |

proton resonance connectivities between heme substituents that are nearest neighbors, such as the heme propionate 7α−7α protons (cross-peak a), heme 2-CH−heme 2-$CH_3$ (cross-peak d), heme 1-$CH_3$−heme 2-$CH_3$ (cross-peak c), and the heme 5-$CH_3$−heme $\beta_{meso}$ proton (cross-peak b).

Figure 4B is the spectrum obtained with a 25 ms mixing time and reveals longer range NOEs. In this figure, the intensity in the diamagnetic region is much greater than in Figure 4A due to relaxation-mediated processes that proceed during this longer mixing time. The complexity of the assignment process was greatly increased at even longer mixing times; however, the procedure remained the same as that for the free form of iso-1-ferricyt *c*. At this longer mixing time (25 ms), longer range NOEs were identified that exhibited the same patterns as those found in corre-

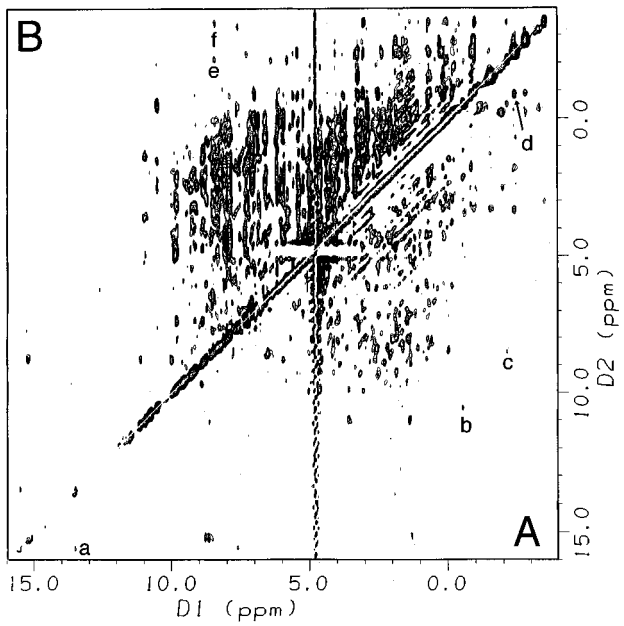


FIGURE 4: Split diagonal 500 MHz contour plot of a $^1$H DEFT−NOESY spectrum of the 46.7 kDa 1:1 noncovalent complex of yeast iso-1-ferricytochrome *c*/CcP in 99.9% $D_2O$ and 10 mM potassium phosphate buffer at pH 6.9 collected at 25 °C. Part A was acquired with a mixing time of 7 ms, and part B was acquired with a mixing time of 25 ms. Cross-peak assignments are described in the text.

sponding spectra of free form iso-1-ferricyt *c*. For example, in the complex, the iso-1 heme 1-$CH_3$ resonance was identified by NOEs to the heme $\delta_{meso}$ proton, to the ring current-shifted heme 2-$CH_3$, and to the ring current-shifted Leu68 $\delta$-$CH_3$. Likewise, the heme $\delta_{meso}$ proton was identified by resolved cross-peaks from the heme 2-$CH_3$ (cross-peak e) and Leu68 $\delta$-$CH_3$ (cross-peak f). Table 1 also summarizes proton assignments for CcP-complexed iso-1-ferricyt *c*.

*Magnetic Axes Determination.* With this catalog of strongly hyperfine-shifted proton resonance assignments, it was possible to consider elucidating the orientations of the principal axis systems of the paramagnetic susceptibility tensors for free and complexed iso-1-ferricyt *c*, as defined by the purely dipolar proton resonance shifts. These orientations describe the fundamental paramagnetic electronic structure of these proteins. One goal of this effort was to determine if complex formation induces any electronic structure change for the iso-1-ferricyt *c* heme. Another goal was to determine if the complex-induced shifts could be accounted for by this type of electronic structure change. The more extensive list of complex-induced shifts that are available from the assignments made here (Table 1) is what makes this effort now possible. The method we have used was developed by Emerson and La Mar (1990) and subsequently applied to myoglobin (Rajarathnam et al., 1992), peroxidases (La Mar et al., 1995), and cyt $b_5$ (Guiles et al., 1996). The general procedure (Emerson & La Mar, 1990) is to fit the observed proton dipolar shifts [$\delta_{dip}$(obs)] to equations describing the magnetic anisotropy using geometrical coordinates and distances derived from the crystal structures (Louie & Brayer, 1990; Pelletier & Kraut, 1992).

*Magnetic Anisotropy in Wild-Type Yeast Iso-1-ferricyt c.* The coordinates for yeast iso-1-ferrocyt *c* (Louie & Brayer, 1990) were used in the magnetic axes determination with the assumption that there are only slight conformational changes upon oxidation (Berghuis & Brayer, 1992). The magnetic axes were determined by three-parameter least-squares searches for $R(\alpha,\beta,\gamma)$, using experimental dipolar shifts for heme vicinity amino acids. Fixed magnetic anisotropies were initially used: $\Delta\chi_{ax} = 1646 \times 10^{-12}$ m$^3$/mol and $\Delta\chi_{rh} = -573 \times 10^{-12}$ m$^3$/mol (Horrocks & Greenberg, 1973). The least-squares searches were subsequently extended to five parameters to determine if a better fit was achieved by varying the $\Delta\chi$s. The results from these searches are as follows. The three-parameter searches yielded the following angles: $\alpha = 250.0°$, $\beta = 5.9°$, and $\gamma = 120°$ ($\kappa = 370°$) with an $F/n$ value of 0.278 ppm$^2$. The extension to five parameters resulted in a decrease in the error function ($F/n = 0.051$ ppm$^2$), minimal changes in the angles ($\alpha = 245.0°$, $\beta = 6.0°$, $\gamma = 135°$, and $\kappa = 380°$), and changes in both the axial anisotropy ($\Delta\chi_{ax} = 2007 \times 10^{-12}$ m$^3$/mol) and the rhombic anisotropy ($\Delta\chi_{rh} = -934 \times 10^{-12}$ m$^3$/mol). These data are summarized in Table 3A, and the orientation of the magnetic axis system for free iso-1-ferricyt *c* is shown in Figure 1B.

Table 3: Magnetic Axes Determination

(A) Yeast Iso-1-ferricyt *c*
$\alpha = 245.0°$, $\beta = 6.0°$, $\gamma = 135.0°$, and $\kappa = 380°$
$\Delta\chi_{ax} = 2007 \times 10^{-12}$ m$^3$/mol and $\Delta\chi_{rh} = -934 \times 10^{-12}$ m$^3$/mol

(B) Yeast Iso-1-ferricyt *c* Complexed with CcP
$\alpha = 40.0°$, $\beta = 9.1°$, $\gamma = 160°$, and $\kappa = 200°$
$\Delta\chi_{ax} = 1646 \times 10^{-12}$ m$^3$/mol and $\Delta\chi_{rh} = -903 \times 10^{-12}$ m$^3$/mol

(C) Yeast Iso-1-ferricyt *c* Complexed with CcP Optimal Fit to Heme Dipolar Shift Pattern
$\alpha = 50.0°$, $\beta = 15.0° \pm 3.0°$, $\gamma = 175°$, and $\kappa = 225°$
$\Delta\chi_{ax} = 1646 \times 10^{-12}$ m$^3$/mol and $\Delta\chi_{rh} = -903 \times 10^{-12}$ m$^3$/mol

The initial input data set for the magnetic axes determination included six protons that had considerable dipolar shifts [i.e. $\delta_{dip}$(obs) $\geq$ 1 ppm]. This data set consisted of the following amino acids: Leu15$\alpha$ [$\delta_{dip}$(obs) = −2.07 ppm], Val28$\alpha$ [$\delta_{dip}$(obs) = 0.93 ppm], Pro30$\delta$ [$\delta_{dip}$(obs) = 4.68 ppm], Leu68$\delta$ [$\delta_{dip}$(obs) = 1.16 ppm], Leu68$\delta$ [$\delta_{dip}$(obs) = 4.23 ppm], and Phe82$\delta$ [$\delta_{dip}$(obs) = 1.27 ppm], where $\delta_{dip}$(obs) is the experimentally determined proton dipolar shift. Using the magnetic axes determined from this initial search, the predicted dipolar shifts ($\delta_{calc}$) were calculated for proton resonances of several other amino acids. These calculated dipolar shifts were used to find and assign several new resonances (Table 1). The additional assignments were then used to recalculate the magnetic axes The results were the same as indicated above, with a similar quality fit (Table 3A). A plot of $\delta_{dip}$(obs) vs $\delta_{calc}$ is predicted to be a straight line of unit slope for a perfect fit, and such plots are thus valuable for assessing the quality of the magnetic axes determination. Figure 5A shows such a plot of $\delta_{calc}$ vs $\delta_{dip}$(obs) for many of the significantly hyperfine-shifted proton resonances assigned for free iso-1-ferricyt *c*. This graph shows a linear correlation to the line drawn to unit slope, indicating that we have reasonably identified the orientation of the magnetic axes and resultant dipolar field.

There are also two sets of resonances that exhibit significant hyperfine shifts yet do not fall on the predicted line (Figure 5B). In Figure 5B, the group of five points (filled boxes) is from residues Thr19, Thr78, Ala81, and Phe82. In a previous determination of **g**-tensor axes for the mutant C102T iso-1-ferricyt *c* (Gao et al., 1991), a similarly poor fit was found for these residues which was attributed

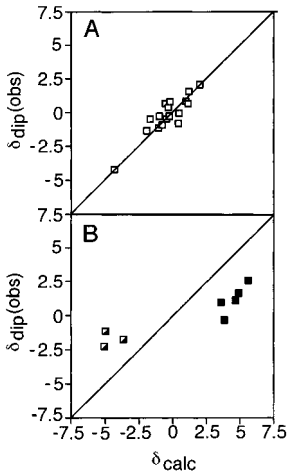


FIGURE 5: (A) Correlation of observed dipolar shifts, $\delta_{dip}$(obs) in parts per million, with dipolar shifts calculated using the magnetic axis orientation shown in Figure 1B, $\delta$(calc) in parts per million, for free wild-type iso-1-ferricyt *c*. (B) Graph similar to part A, showing exceptions to the correlation, as discussed in the text.

either to a difference in the structure between the solution and solid state or to changes in localized structure upon oxidation of cyt *c*. The group of three points (half-filled boxes) arises from Val28$\gamma$, Tyr46$\epsilon$, and Leu68$\delta$. The source of deviation for Val28 likely comes from the fact that it is also in a region whose structure is affected upon oxidation (Gao et al., 1991; Berghuis & Brayer, 1992). Thus, our use of the wild-type iso-1-ferrocyt *c* coordinates is likely to be a source of error for protons from Val28, as well as those from Thr19, Thr78, Ala81, and Phe82. In the case of Tyr46$\epsilon$ and one of the Leu68 $\delta$-methyl groups, the deviation could be due to motional averaging, due to ring flipping (Tyr46), or, for Leu68 $\delta$-methyl interconversion, due to rotation about the C$\gamma$−C$\beta$ bond. In this type of rotational averaging, prochiral protons are in fast exchange, with averaged positions and chemical shifts, not reflected in the static crystal structure.

Our magnetic susceptibility axis system orientation for free iso-1 (Table 3; indicated by *x*,*y*,*z* in Figure 1B) is comparable to previous **g**-tensor axes determinations from NMR data (Feng et al., 1990; Gao et al., 1991). For horse ferricyt *c*, Feng et al. (1990) found $\kappa$ (=$\alpha$ + $\gamma$) = 353° (see Figure 1 for definitions) and for the C102T variant of yeast iso-1-ferricyt *c*, Gao et al. (1991) found $\kappa$ = 366°. A $\kappa$ angle of 360° means that $g_x$ ($\chi_{xx}$) and $g_y$ ($\chi_{yy}$) are aligned along the diagonal heme nitrogens (*X*′ and *Y*′) as shown in Figure 1. Our $\kappa$ of 380° (Figure 1B; *X* and *Y*) is slightly larger than the previous determinations but indicates that $\chi_{xx}$ and $\chi_{yy}$ are generally oriented in this same way. The angle $\beta$, which represents the deviation of $\chi_{zz}$ from the heme normal, as defined by the Fe−N(His18) bond (Figure 1D), is often the most susceptible to subtle structural changes, and our value of 6° is close to the 9° value reported for the determination of $g_z$ for C102T iso-1 (Gao et al., 1992) and the 10° value found in the crystal structure (Louie & Brayer, 1990).

It is interesting that although the data developed by paramagnetic susceptibility anisotropy equations and **g**-tensor anisotropy equations for the dipolar shifts have produced seemingly analogous results for the wild-type and variant iso-1-ferricyt *c* this may be fortuitous. Strictly speaking for ferricyt *c*, it is not possible to determine a unique ground state **g**-tensor from NMR data because ferricyt *c* possesses a degenerate orbital ground state. Therefore, we prefer to interpret the **g**-tensor data as indicating the general symmetry of the paramagnetic dipolar field, and in this respect, the two data sets are similar.

*Magnetic Susceptibility Axes for CcP-Bound Iso-1-ferricyt c.* The crystal structure for the 1:1 yeast iso-1-ferricyt *c*/CcP complex, which has been determined to 2.3 Å resolution (Pelletier & Kraut, 1992), served as the structural basis for this determination. As before, purely dipolar-shifted amino acid protons for iso-1-ferricyt *c* in the solution complex, along with the crystal coordinates for iso-1 in the solid state complex, were used as initial input data for the three-parameter least-squares searches for $R(\alpha,\beta,\gamma)$ using the initial magnetic anisotropies and paramagnetic tensor axes orientations of Horrocks and Greenberg (1973).

As noted above, the large size of the complex engendered large proton resonance density, which severely limited unambiguous assignments of purely dipolar-shifted resonances to nine resonances that were also assigned for free iso-1 (Table 1). When all nine of these resonances were used to fit the magnetic axis orientation, a very poor result was found, as judged by the large error function (*F*/*n*) of 650 ppm$^2$. However, using a subset of five of those nine assigned resonances, a three-parameter fit was found to yield a much improved error value of 2.96 ppm$^2$. The Euler angles that defined the paramagnetic susceptibility axis system orientation for this result are given in Table 3B, and the axes orientations are depicted graphically in Figure 1C. The error function for this result is still larger than that found for free iso-1-ferricyt *c* and must be partly attributed to the small basis set of assigned resonances. Although smaller error might occur with a larger set of assigned resonances, the experiments presented here represent the current limits of our capability with available technology and economic resources. In the near future, expanded assignments for this complex are therefore unlikely. Further, there is no guarantee that more assignments would improve these results since the poorer fit achieved with the larger assignment set here implies that the complex crystal structure does not serve as an accurate structural basis for fitting the magnetic axis system to the experimental dipolar shifts. This result further suggests that there are significant structural differences between iso-1-ferricyt *c* free in solution and complexed to CcP.

## DISCUSSION

*The General Pattern of Complex-Induced Shifts for Protons of Heme Peripheral Substituents Can Be Described by Changes in Magnetic Axis System Orientation.* As reported in Table 1, complex-induced shifts for protons of nearly all heme peripheral substituents have been made. This comprehensive mapping of complex-induced shifts, extending over 80% of the heme periphery, allowed us to have an alternative evaluation of the appropriateness of the magnetic axis orientation derived for iso-1 in the complex (Figure 1C, Table 3B). The approach taken was to determine whether any magnetic axis system orientation for complexed iso-1 could reproduce the irregular pattern of complex-induced shifts for the iso-1-ferricyt *c* heme protons.

We understand that the observed proton shifts for the heme peripheral substituents are dominated by the contact term in the hyperfine-shift equations (La Mar & Walker, 1974;

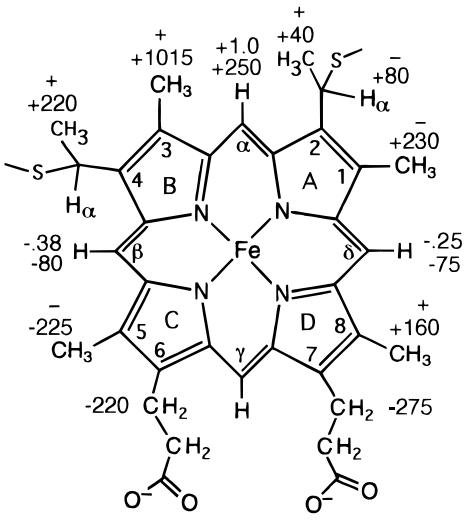


FIGURE 6: Heme *c* structure showing the complex-induced shifts for the assigned resonances of the peripheral substituent protons. The lower numbers reflect the observed complex-induced shifts. Signs shown above each number indicate the direction of the calculated proton dipolar complex-induced shift (+ indicates downfield or high frequency; − indicates upfield or low frequency). For the three assigned heme meso-proton positions, the calculated complex-induced relative numerical magnitudes are shown in addition to their directions.

Satterlee, 1986), indicating strong dependence on delocalized unpaired spin density in the heme orbitals. But the magnitudes of the individual, experimentally observed complex-induced shifts are less than or equal to approximately 7% of the total observed shift magnitude for any heme proton (Table 1). Therefore, the experimentally observed complex-induced shifts could be wholly due to slight changes in the magnetic axis-dependent dipolar term in the hyperfine-shift equation (La Mar & Walker, 1974; Satterlee, 1986). It was felt that if the observed complex-induced shifts were due to the difference in magnetic axis system orientation for free and complexed iso-1-ferricyt *c* then the calculated dipolar complex-induced heme proton shifts should have the same pattern (but not necessarily the same magnitudes) as the experimentally observed complex-induced shifts.

The experimentally observed complex-induced shift for a given proton, $\delta_{c-i}$(obs), is defined as the difference in observed proton resonance shifts between the complexed and free forms of iso-1-ferricyt *c* (Table 1; expressed in hertz at 500 MHz):

$$\delta_{c-i}(\text{obs}) = \delta_{\text{complex}}(\text{obs}) - \delta_{\text{free}}(\text{obs}) \qquad (5)$$

The experimentally determined numerical values of $\delta_{c-i}$(obs) for each assigned heme proton have been labeled on the heme structure shown in Figure 6. The direction of each shift is indicated by + and − signs. Positive shifts are downfield (to high frequency), while negative shifts are upfield (low frequency).

To complete this comparison, we had to perform the calculations equivalent to eq 5, but using dipolar shifts for each heme proton calculated (i.e. predicted) from specific magnetic axis system orientations as input data. That is, we had to evaluate eq 6,

$$\delta_{\text{dip}/c-i}(\text{calc}) = \delta_{\text{dip/complex}}(\text{calc}) - \delta_{\text{dip/free}}(\text{calc}) \qquad (6)$$

for each heme proton for free and complexed iso-1.

Since the magnetic axis system for free iso-1 is well defined, only one orientation was used (Table 3A), and the result of the calculation gave $\delta_{\text{dip/free}}$(calc) for each heme proton. For iso-1 complexed to CcP, we calculated an array of values for $\delta_{\text{dip/complex}}$(calc) (for each heme proton) by varying the magnetic axes orientations by altering the Euler angles as follows: $\alpha$ (0−360°), $\beta$ (6−18°), and $\gamma$ (100−360°). The initial values for this search were those given in Table 3B.

The results of the calculations represented by eqs 5 and 6 were then compared. The criterion for evaluation was to identify Euler angles (i.e. axis orientations employed in calculations of the first term on the right in eq 6) which maximized the agreement between the experimentally observed complex-induced shift (eq 5) and the calculated dipolar complex-induced shift (eq 6) for the assigned heme protons. The results (Table 3C, Figure 1D) revealed that there is a family of Euler angles closely related to those derived from the three-parameter fit (Table 3B, Figure 1C) which, when employed in eq 6 to calculate $\delta_{\text{dip}/c-i}$(calc), accurately reproduce the directions of experimentally observed heme proton complex-induced shifts.

The $\delta_{\text{dip}/c-i}$(calc) shift-direction pattern for one of these results (optimal fit, Table 3C) is represented in Figure 6 as + and − signs above the numerical values of the observed complex-induced shifts. For the three assigned heme meso protons, we have also included in Figure 6 the relative $\delta_{\text{dip}/c-i}$(calc) shift magnitudes (normalized to the $\alpha$-meso shift). They are presented above the experimentally observed complex-induced shift numbers.

The agreement between patterns of observed complex-induced shifts and calculated dipolar complex-induced shifts is quite good, with only two positions, the 1-$CH_3$ and 2-$\alpha$H, in disagreement. Furthermore, taken as a subset, the data for the three assigned heme meso protons ($\alpha$, $\beta$, amd $\delta$, Figure 6) are in agreement *in sign* and *in relative magnitude*, with both observed and calculated complex-induced shifts for the $\alpha$ position showing a large positive shift and the $\beta$ and $\delta$ positions showing small negative shifts.

The Euler angles found for the optimal fit to the heme shifts (Table 3C, Figure 1D) and the original three-parameter fit to the purely dipolar shifts (Table 3B, Figure 1C) are very similar. This lends credibility to the concept that complex formation alters the iso-1-ferricyt *c* magnetic susceptibility axis system orientation. Further support for such a complex-induced electronic perturbation comes from the fact that $\delta_{\text{dip}/c-i}$(calc) is very sensitive to Euler angles and the fact that agreement between calculated and observed complex-induced shifts for the heme proteins decreased substantially (decreasing pattern matches) as the Euler angles deviated by more than ±25° from the values reported for the optimal fit (Table 3C). This indicates that the heme dipolar shifts are highly discriminating.

*The Angle $\beta$ Increases upon Complex Formation.* This angle defines the deviation of $\chi_{zz}$ (*Z*) from the approximate heme normal (*Z*′) which is defined by the Fe−N(His18) bond (Figure 1E). In free iso-1-ferricyt *c*, it is a well-defined 6°. In the complex, $\beta$ increases to 9.1° (Table 3B) or to as much as 18° (Table 3C), depending upon the specific fitting procedure employed. Regardless of the uncertainty in the numerical value of the angle change, all of these results suggested that $\beta$ increased upon complex formation. Such an increase apparently has no structural manifestation in the

solid state. In the complex crystal structure (Pelletier & Kraut, 1992), the (Met80)S−Fe−N(His18) axial ligand angle is 9°, and essentially unchanged from the 10° value measured for free iso-1-ferrocyt *c*.

*Localized Factors Also Contribute to the Complex-Induced Shift.* This conclusion comes from two pieces of data. First, the largest observed complex-induced proton shift is 1015 Hz for the heme 3-$CH_3$ resonance. This is about 5 times larger than the magnitudes found for the other five heme methyl resonances (Figure 6). Interestingly, it is also about 5 times larger than its nearest neighbors on the heme ring, the $\alpha_{meso}$-H and the 4-($\beta$)$CH_3$. Additionally, then, there must be a specific structural or electrostatic interaction accompanying complex formation with CcP that specifically alters the iso-1-ferricyt *c* 3-$CH_3$ environment compared to its neighbors.

With CcP being net negatively charged at pH 6.4, it is hard to see how this large, specific downfield shift could be due to a general effect of CcP complexation, say by a "polyanion" or electrostatic effect. However, it could be due to complex-induced movement of a positively charged iso-1 surface amino acid, such as lysine or arginine, closer to the 3-$CH_3$, but not its neighbors. We note that in this respect the position-13 amino acid is one of the distinguishing primary sequence differences between yeast iso-1-cyt *c* and either horse or tuna cyt *c*. Iso-1 has an Arg13, while in the other two cyt *c*s, it is Lys13. We note that in NMR comparisons of the observed complex-induced shift of the 3-$CH_3$ resonance of each of these three different species the iso-1/CcP shift is ∼5 times larger than for the other two, suggesting a unique magnetic environment change for the iso-1 heme 3-$CH_3$ (Moench et al., 1992). The essence of these ideas has been expressed in detail previously (Falk & Angstrom, 1983; Satterlee et al., 1987; Moench et al., 1992) and remains consistent with the current data.

Similarly, the anomalous complex-induced shift direction for the heme 1-$CH_3$ resonance and its neighboring 2-αH resonance (Figure 6) are probably manifestations of a localized structure change that offsets the dipolar complex-induced shift. We conclude that, although the gross changes identified as complex-induced shifts are accountable by paramagnetic susceptibility changes, there are also localized structure changes at the heme that alter the heme substituent magnetic environment, either directly or by mediation of unpaired spin density delocalization.

*Implications for Electron Transfer.* Analysis of the complex crystal structure (Pelletier & Kraut, 1992) identified only one major conformational change in iso-1-ferricyt *c* caused by complexation. It was found that the side chain of Gln16 folded back to form a hydrogen bond with its own backbone amide nitrogen, thereby exposing the ferricyt *c* pyrrole ring B (Figures 1 and 6). In the crystal structure of the complex, the iso-1-ferricyt *c* heme 4-$CH_3$ is in closest contact with CcP (Pelletier & Kraut, 1992). The NMR data agree with the idea that the iso-1 heme *c*'s pyrrole ring B vicinity is the most affected by complexation, not only by the unusually large heme 3-$CH_3$ complex-induced shift (1015 Hz) but also by observed complex-induced shifts for protons of nearby amino acids, as well. In this region, Phe82-, Pro30-, and Gly29-assigned protons experience significant complex-induced shifts (Table 1), which agrees with previously determined H/D protection factors that helped define the CcP/iso-1-cyt *c* interaction interface in solution (Yi et al., 1994).

The complex crystal structure and accumulated solution NMR studies on the complex all identify the same region of wild-type iso-1-ferricyt *c* as the primary interaction interface with CcP in the 1:1 complex. However, the electron transfer active complex involves ferrocyt *c*, and an outstanding question concerns the implications of these results for the active redox complex. One answer to this question is that the ferricyt *c* studies reveal that interaction with CcP affects yeast iso-1-cyt *c* more than superficially. The iso-1-ferricyt *c* results presented here indicate that CcP can affect the heme electronic structure (magnetic axes orientations) perhaps by a comprehensive, but subtle, structural change. Superimposed upon this effect are further highly specific structural rearrangements. The clear impression left by these studies is that CcP "polarizes" the structural and electronic properties of ferrocyt *c* so as to facilitate electron transfer from the pyrrole B edge of heme *c*.

## ACKNOWLEDGMENT

We thank Professor Gerd N. La Mar for kindly making available for our use his suite of programs for locating the paramagnetic susceptibility tensor axis system. We gratefully acknowledge use of the Protein Data Bank.

## REFERENCES

Baistrocchi, P., Banci, L., Bertini, I., & Turano, P. (1996) *Biochemistry 35*, 13788−13796.
Berghuis, A. M., & Brayer, G. D. (1992) *J. Mol. Biol. 223*, 959−976.
Bernstein, F. C., Koetzle, T. F., Williams, G. J. B., Meyer, E. F., Jr., Brice, M. D., Rodgers, J. R., Kennard, O., Shimanouchi, T., & Tasumi, M. (1977) *J. Mol. Biol. 112*, 535−542.
Bertini, I., Luchinat, C., & Tarchi, D. (1993) *Chem. Phys. Lett. 203*, 445−449.
Cross, K. J., & Wright, P. E. (1985) *J. Magn. Reson. 64*, 220−231.
Emerson, S. D., & La Mar, G. N. (1990) *Biochemistry 29*, 1556−1566.
Falk, K. E., & Angstrom, J. (1983) *Biochim. Biophys. Acta 772*, 291−296.
Feng, Y., Roder, H., & Englander, S. W. (1990) *Biochemistry 29*, 3493−3504.
Gao, Y., Boyd, J., Peilak, G. J., & Willliams, R. J. P. (1991) *Biochemistry 30*, 1928−1934.
Gao, Y., McLendon, G., Pielak, G. J., & Williams, R. J. P. (1992) *Eur. J. Biochem. 204*, 337−352.
Griesinger, C., Otting, G., & Wuthrich, K. (1988) *J. Am. Chem. Soc. 110* , 7870−7872.
Guiles, R. D., Siddahartha, S., DiGate, R. J., Banville, D., Basus, V. J., Kuntz, I. D., & Waskell, L., (1996) *Nat. Struct. Biol. 3*, 333−339.
Hahm, S., Miller, M. A., Geren, L., Kraut, J., Durham, B., & Millet, F. (1994) *Biochemistry 33*, 1473−1480.
Horrocks, W. D., Jr., & Greenberg, E. S. (1973) *Biochim. Biophys. Acta 322*, 38−44.
IUPAC-IUB (1988) *Eur. J. Biochem. 178*, 277−328.
Kao, L. F., & Hruby, V. J. (1986) *J. Magn. Reson. 70*, 394−407.
La Mar, G. N., Chen, Z., Vyas, K., & McPherson, D. (1995) *J. Am. Chem. Soc. 117*, 411−419.
Liu, R. Q., Hahm, S., Miller, M. A., Durham, B., & Millet, F. (1995) *Biochemistry 34*, 973−983.
Louie, G. V., & Brayer, G. D. (1990) *J. Mol. Biol. 214*, 527−555.
Matthis, A., & Erman, J. E. (1995a) *Biochemistry 34*, 9985−9990.
Matthis, A., Vitello, L. B., & Erman, J. E. (1995b) *Biochemistry 34*, 9991−9999.
Mauk, M. R., Ferrer, J. C., & Mauk, A. G. (1994) *Biochemistry 33*, 12609−12614.

Miller, M. A., Geren, L., Han, G. W., Saunders, A., Beasley, J., Pielak, G. J., Durham, B., Millett, F., & Kraut, J. (1996) *Biochemistry 35*, 667−673.
Moench, S. J., & Satterlee, J. D. (1989) *J. Biol. Chem. 264*, 9923−9931.
Moench, S. J., Chroni, S., Lou, B.-S., Erman, J. E., & Satterlee, J. D. (1992) *Biochemistry 31*, 3661−3670.
Neuvo, M. R., Chu, H. H., Vitello, L. B., & Erman, J. E. (1993) *J. Am. Chem. Soc. 115*, 5873−5874.
Papa, H. S., & Poulos, T. L. (1995) *Biochemistry 34*, 6573−6577.
Pelletier, H., & Kraut, J. (1992) *Science 258*, 1748−1755.
Pielak, G. J., Boyd, J., Moore, G. R., & Williams, R. J. P. (1988) *Eur. J. Biochem. 177*, 167−177.
Poulos, T. L., & Finzel, B. C. (1984) *Pept. Protein Rev. 4*, 115−172.
Qin, J., Delaglio, F., La Mar, G. N., & Bax, A. (1993) *J. Magn. Reson., Ser.B102*, 332−336.
Rajarathnam, K., La Mar, G. N., Chiu, M. L., & Sligar, S. G. (1992) *J. Am. Chem. Soc. 114*, 9048−9058.
Satterlee, J. D. (1986) In *Annual Reports on NMR Spectroscopy* (Webb, G. A., Ed.) Vol. 17, pp 79−178, Academic Press, London.
Satterlee, J. D., Moench, S. J., & Erman, J. E., (1987) *Biochim. Biophys. Acta 912*, 87−97.
Satterlee, J. D., Moench, S. J., & Avizonis, D. (1988) *Biochim. Biophys. Acta 952*, 317−324.
States, D. J., Haberkorn, R. A., & Ruben, D. J. (1992) *J. Magn. Reson. 68*, 286−292.
Stemp, E. D. A., & Hoffman, B. M. (1993) *Biochemistry 32*, 10848−10865.
Sukits, S. F., & Satterlee, J. D. (1996) *Biophys. J. 71*, 2848−2856.
Vitello, L. B., Huang, M., & Erman, J. E. (1990) *Biochemistry 29*, 4283−4288.
Wishart, D. S., Sykes, B. D., & Richards, F. M. (1991) *J. Mol. Biol. 222*, 311−333.
Yi, Q., Erman, J. E., & Satterlee, J. D. (1994) *Biochemistry 33*, 12032−12041.
Zhou, J. S., & Hoffman, B. M. (1994) *Science 265*, 1693−1696.

BI970072B